JOURNAL OF SOLID STATE CHEMISTRY 46, 121–131 (1983)

Orientation and Thickness Corrections for Two-Dimensional Polycrystals

M. UDA AND Y. SASA

The Institute of Physical and Chemical Research, Wako-shi, Saitama, Japan

Received July 22, 1982

X-Ray and electron diffraction intensities are well explained by use of the Gaussian function for two-dimensionally oriented polycrystals. Diffraction intensities for thin films with preferred orientation are also well understood by this treatment if coupled with a thickness correction factor, $1/\sin\theta$. Examples are given for MoO_3, α-Fe_2O_3, $CaSO_4 \cdot 2H_2O$, $SmCo_5$, BN, MoS_2, SnO, NiO, and thin films of Al, Ag, Au, and Cd.

I. Introduction

The *R* factor used for the structure analysis should be smaller in the polycrystalline method than in the single-crystal method because one and the same reflection results from a series of (*hkl*) planes in the former, and one reflection comes from only one corresponding (*hkl*) plane in the latter. However, this is indeed not the case in general. Such an inexpedient result is mainly caused by the preferred orientation of polycrystalline aggregates. The pole figure method has been used for the analysis of the preferred orientation, but this needs a specially designed sample holder and considerable experience. A simple method for estimating the degree of orientation has been proposed by Lotgering (*1*), in which a ratio of diffracted intensities from oriented and ideally dispersed polycrystallites is used. However, this method does not give the crystalline orientation itself.

One of the authors (M.U.) (*2, 3*) has attempted to analyze the degree of orientation quantitatively by use of a distribution function. Two-dimensional platy crystallites have their well-developed planes aligned almost parallel to the plane of the sample supporting film for transmission electron diffraction. The method has also been applied to the X-ray structure analysis of USi_2 (*4*) for which neither a single crystal of appreciable size nor ideally powdered crystals can be obtained.

In this report the general applicability of the method for two-dimensionally oriented polycrystals will be verified experimentally, and several practical examples will be given. Thin films with preferred orientations will also be treated here for the first time.

II. Analytical Method

X-Ray diffraction intensities for polycrystals with random orientations are given by

$$I_{hkl}^{\text{ideal}} = A \cdot |F_{hkl}|^2 \cdot Lp \cdot p, \qquad (1)$$

where A is a numerical constant including the absorption coefficient, F_{hkl} is the structure amplitude including the Debye–Waller

0022-4596/83/010121-11$03.00/0

temperature factors, L_p is Lorentz-polarization factor, and p is the multiplicity factor. In the case of electron diffraction, L_p is replaced by d^2, where d is an interplanar spacing.

Equation (1) cannot be directly applied to oriented polycrystals. In such a case, one must correct Eq. (1) by taking a term responsible for orientation into account. Although there are many types of deviation from randomness, let us confine ourselves here to the uniaxially anisotropic or two-dimensional orientation.

When aggregates of uniaxially oriented polycrystals are packed into the welled sample holder, the aggregates tend to align their well-developed plane parallel to the plane of the holder (hereafter the well-developed plane will be called the orientation plane). Now, let us make an assumption that the distribution of the uniaxially oriented polycrystallites is expressed in terms of the Gaussian function $\exp(-h_0^2 \cdot \phi_{hkl}^2)$, where h_0 is a Gaussian constant representing a degree of preferred orientation and ϕ_{hkl} is a plane angular component defined by the solid angle made by normals of both the orientation plane and the quoted hkl plane. Thus the diffraction intensities of the uniaxially oriented polycrystallites can be expresed as

$$I_{hkl}^{\mathrm{pref}(1)} = I_{hkl}^{\mathrm{ideal}} \exp(-h_0^2 \cdot \phi_{hkl}^2). \quad (2)$$

When the aggregates possess high crystal symmetry, the plane angular components for one set of the equivalent Miller indices are not always restricted to the single one. In this case, all intensities emitted from the planes with the same value of ϕ_{hkl} are summed up by taking into account the multiplicity factors.

Strictly speaking, Eq. (2) is applicable only to the case with a unique and uniform degree of orientation throughout the specimen. However, this is usually not the case. On being subjected to pressure, the platy crystallites tend to form oriented aggregates. The stress is developed to maximum value at the surface of the specimen contacted with a pressing tool, and relaxes toward the inner parts of the specimen. Then the degree of orientation varies as a function of location for individual crystallites, and Eq. (2) should be replaced by

$$I_{hkl}^{\mathrm{pref}(2)} = I_{hkl}^{\mathrm{ideal}} \iiint \exp[-h^2(x,y,z) \cdot \phi_{hkl}^2] dxdydz. \quad (3)$$

In practice, it is very difficult to estimate the upper limits of the integrals and to define the type of funtion $h(x,y,z)$. Now Eq. (3) might be divided, as a matter of convenience, into two terms,

$$I_{hkl}^{\mathrm{pref}} = I_{hkl}^{\mathrm{ideal}}[b + (1 - b)\exp(-h^2 \cdot \phi^2{}_{hkl})], \quad (4)$$

where b is a constant responsible for randomness retained at such regions as edges and the inner parts of the sample where molding pressure could not be attained, and $(1 - b)\exp(-h^2 \cdot \phi_{hkl}^2)$ is a mean distribution function appropriate everywhere except for the regions mentioned above. Equation (4) is reduced to Eq. (1) if $h = 0.0$ or $b = 1.0$. Hence h and b are parameters representing the degree of orientation of crystallites. Hereafter we call such an analytical treatment based upon two-dimensional orientation a Texture Pattern Technique (T.P.T.).

Equations (1)–(4) hold for the specimen with sufficient thickness. With such a specimen the diffracting volume for each reflection is independent of the Bragg angle θ. On the other hand, when the specimen has a thickness insufficient to the penetration depth of the incident X-ray beam, the diffracting volume for each reflection is varied as a function of the Bragg angle, as shown in Fig. 1. The higher the Bragg angle takes, the smaller the diffracting volume. The rate of variation is proportional to $1/\sin\theta$. Then the diffraction intensities for the random aggregates with incomplete thickness are

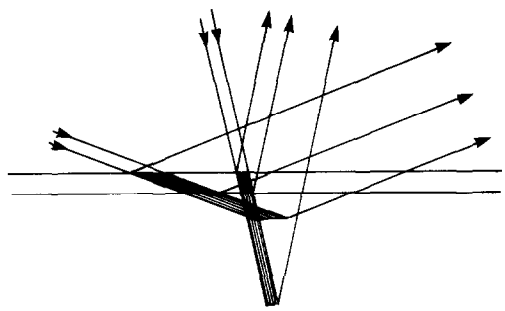

FIG. 1. Thickness effect on diffraction volume. When a specimen has a thickness insufficient to the penetration depth of incident X rays, the irradiated volume of the specimen by X rays changes with 1/sin θ.

given by

$$I_{hkl}^{ideal'} = I_{hkl}^{ideal}/\sin\theta, \quad (5)$$

and for the uniaxially oriented aggregates the intensities are,

$$I_{hkl}^{pref'} = I_{hkl}^{ideal}[b + (1 - b)\exp(-h^2 \cdot \phi_{hkl}^2)]/\sin\theta. \quad (6)$$

III. Experimental

An X-ray diffraction analysis was made with the use of a powder diffractometer equipped with the graphite monochromator for Cu$K\alpha$ radiation and the scintillation counter. Integrated intensities of every reflection were recorded digitally with the step scan mode or graphically with the continuous scan mode. The operation of the former was performed under the condition of a step increment of $2\theta = 0.02°$ and counting time of 10 sec. For the latter mode a goniometer speed of 0.125°/min and a time constant of 5 sec were adopted.

Electron diffraction analysis was made under an accelerating voltage of 50 keV. The diffraction intensities recorded on the photographic films were measured visually.

The diffraction intensities for the polycrystals with random orientation were calculated based on the single-crystal data given by the references. All of the calculations were executed on a FACOM-230-75 computer with the use of the modified program of the UNICS (*5*).

IV. Results and Discussions

1. Attempt To Reduce the Preferred Orientation Effect through Sample Preparation

Figures 2a–d show the schematic X-ray diffraction patterns for orthorhombic MoO_3 polycrystals. The top panel illustrates an ideal diffraction pattern for randomly oriented MoO_3 polycrystals whose intensities were calculated by use of Kihlborg's single-crystal data (*6*). The second pattern (b) was taken from MoO_3 powders pressed into the welled sample holder with 0.2 mm thickness. Though the observed and calculated

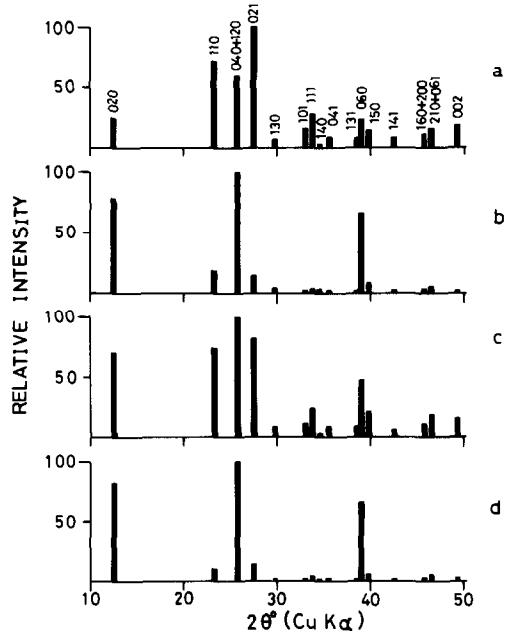

FIG. 2. Schematic X-ray diffraction patterns for MoO_3. (a) Calculated intensities for ideally dispersed powders, R = 1.34 and 0.28, compared with (b) and (c), respectively; (b) observed intensities for pressed MoO_3 powders; (c) observed intensities for the mixture of MoO_3 and silica gel; and (d) calculated intensities for preferentially oriented MoO_3 powders with h = 0.045 and b = 0.05, R = 0.08 compared with (b).

interplanar spacings agree well with each other, the observed relative intensities are much different from ideal ones: the relative intensities of $0k0$ reflection, I_{0k0}, were especially enhanced in the former. Consistency of the observed intensity data with that of the ideal powder can be evaluated in terms of the R factor used in the structure analysis, where $R = \Sigma|I^{obs} - I^{calc}|/\Sigma I^{obs}$. The nonsensically large R value of 134% came from the above data.

A mixture of MoO_3 and silica gel (double weight of MoO_3) was placed in the sample holder applying as light a force as possible. The most intense reflection of this pattern is not the 021 reflection but still 040, although Fig. 2c taken from the specimen resembles somewhat better the ideal powder pattern. The R factor was 28%. Elimination of the preferred orientation effect is still insufficient.

2. Elimination of the Preferred Orientation Effect by the Analytical Method

The diffraction data shown in Fig. 2a and b for MoO_3 were treated with the analytical method of the T.P.T. by examining the curves of Fig. 3 with the aid of Eq. (4). Even for MoO_3 mixed with silica gel we see orientation in the diffraction pattern. We get the values of $h = 0.04$ and $b = 0.05$ as an orientation degree for pure MoO_3. However, such a graphical method is still incomplete as a means for estimating the correct orientation degree: omission of a weighting scheme on intensity data and the presence of overlapped reflections may bring an uncertainty into the estimation of the degree of orientation. Then a set of h and b was determined by comparing I^{obs} and I^{pref} so as to minimize the R factor. From the data for the MoO_3 monophase specimen, the R factor of 7.9% was obtained when $h = 0.045$ and $b = 0.05$ were adopted in Eq. (4). Calculated diffraction intensities are schematically shown in Fig. 2d. A similar result was

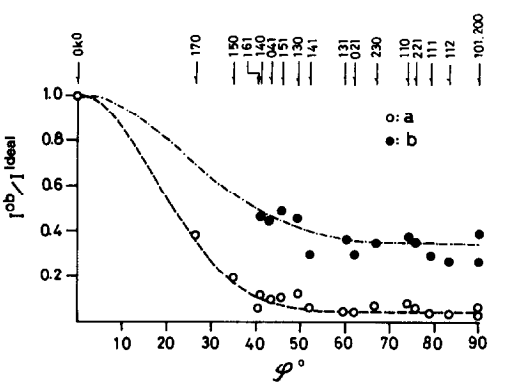

FIG. 3. Observed and calculated intensity ratios (X-ray diffraction) against φ_{hkl}, a plane angular component defined by the solid angle made by normals of both orientation plane and the quoted hkl plane. (a) For pressed MoO_3 with $h = 0.040$ and $b = 0.05$, and (b) for the mixture of MoO_3 and silica gel with $h = 0.030$ and $b = 0.35$.

attained for the mixed specimen of MoO_3 and silica gel: $R = 9.0\%$ at $h = 0.030$ and $b = 0.40$. Table I shows the diffraction data for the MoO_3 monophase sample. Large discrepancies are found between I^{obs} and I^{ideal}, but the differences between I^{obs} and I^{pref} are reduced to reasonable values for every reflection.

Let us check whether or not the T.P.T. holds in general for the two-dimensional aggregates. For this, reflection and transmission electron diffraction were performed on a thin film of α-Fe_2O_3, which was made on a pure iron plate heated at 600°C for several seconds. For transmission electron diffraction, the oxide film was stripped off from the substrate by immersing it in a Br–methanol solution. Interplanar spacings observed from both types of diffraction patterns, as shown in Figs. 4 and 5, agreed well with each other, but the intensity distributions were quite different. On the first inspection of these patterns, $h00$ and $00l$ planes, which are perpendicular with each other, are the orientation planes for the reflection and transmission types of diffraction, respectively. The R factors of 15 and

TABLE I

X-RAY DIFFRACTION DATA ON MoO_3

$h\,k\,l$	d^{obs} (Å)	$d^{calc\,a}$ (Å)	I^{obs}	I^{ideal}	I^{pref} ($h = 0.045$, $b = 0.05$)
0 2 0	6.937	6.9275	78.2	28.9	81.2
1 1 0	3.814	3.8100	17.5	71.7	10.1
0 4 0	3.468	3.4638	100.0	34.4	96.5
1 2 0		3.4398		24.5 → 58.9	3.5 → 100.0
0 2 1	3.264	3.2612	13.8	100.0	14.2
1 3 0	3.011	3.0074	2.6	6.9	1.1
1 0 1	2.705	2.7030	1.8	16.0	2.2
1 1 1	2.653	2.6530	3.4	27.9	3.9
1 0 4	2.609	2.6079	1.0	2.9	0.7
0 4 1	2.531	2.5275	2.2	7.6	1.5
1 2 1	—	2.5181	—	0.9	0.1
1 3 1	2.333	2.3328	1.1	8.6	1.2
0 6 0	2.310	2.3092	66.1	23.1	64.9
1 5 0	2.272	2.2709	8.3	14.5	5.3
1 4 1	2.1315	2.1310	1.6	8.5	1.3
1 6 0	1.9960	1.9952	3.0	2.0	1.1
2 0 0	1.9811	1.9814		9.1 → 11.1	1.3 → 2.4
2 1 0	1.9592	1.9614	5.1	8.2	1.2
0 6 1		1.9584		8.3 → 16.5	4.0 → 5.2
1 5 1	1.9360	1.9349	0.3	1.0	0.2
2 2 0	1.905	1.9050	0.2	0.7	0.1
0 0 2	1.8486	1.8482	1.8	18.7	2.6
2 3 0	1.8211	1.8209	2.3	11.3	1.6
0 2 2	1.7862	1.7857	0.3	1.7	0.2
1 7 0	1.7710	1.7707	2.4	2.1	1.6
1 6 1	1.7565	1.7557	0.9	4.8	1.1
2 1 1	1.7326	1.7326	3.3	16.6	2.3
0 8 0		1.7319		0.3 → 16.9	0.9 → 3.2
2 4 0	1.7193	1.7199	0.5	2.0	0.3
2 2 1	1.6934	1.6934	1.2	6.8	1.0
1 1 2	1.6634	1.6629	1.3	13.7	1.9
2 3 1	1.6337	1.6335	2.0	2.6	0.4
0 4 2	1.6311	1.6036		8.0 → 16.3	1.1 → 2.3
1 2 2	1.6279	1.6281		5.7	0.8
1 7 1	1.5973	1.5969	8.2	15.1	5.0
1 8 0	1.5878	1.5869		2.6 → 19.6	2.6 → 7.9
1 3 2	1.5752	1.5746		1.9	0.3
0 8 1	1.5688	1.5683	9.7	14.1	12.4
2 4 1	1.5597	1.5594		0.5 → 14.6	0.1 → 12.5
R factor				1.336	0.079

[a] $a = 3.9628$, $b = 13.855$, $c = 3.6964$ Å.

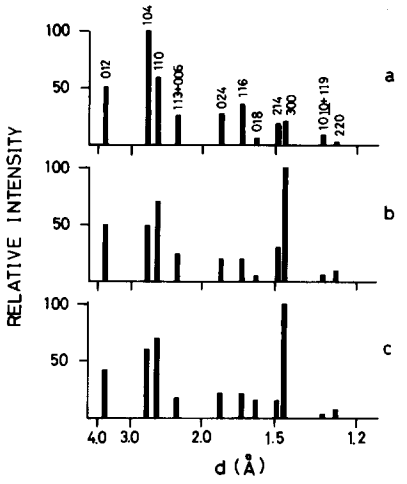

FIG. 4. Reflected electron diffraction patterns for α-Fe_2O_3. (a) Calculated intensities for ideally dispersed crystallites (*8*), $R = 0.50$ compared with (b); (b) observed intensities; and (c) calculated intensities for preferentially oriented ones with $h = 0.053$ and $b = 0.05$, $R = 0.15$ compared with (b).

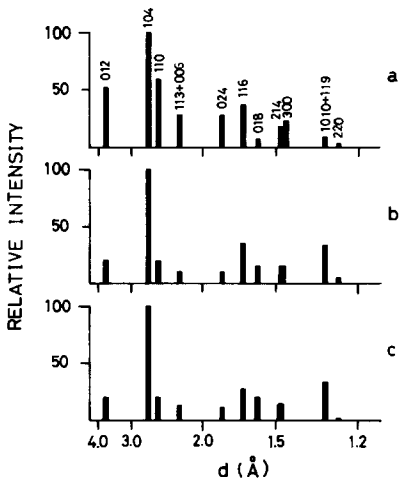

FIG. 5. Transmitted electron diffraction patterns for the same sample used in Fig. 4. (a) Calculated intensities for ideally dispersed powders, $R = 0.66$ compared with (b); (b) observed intensities; and (c) calculated intensities for preferentially oriented α-Fe_2O_3 with $h = 0.040$ and $b = 0.05$, $R = 0.09$ compared with (b).

9% were obtained if we chose $h = 0.053$ and $b = 0.05$ and $h = 0.040$ and $b = 0.05$ for these patterns, respectively. The agreement between observed and calculated intensities is satisfactory if we take into account that the observed intensities were estimated visually. The discrepancy in the h factors can, however, be explained as follows. The coherent scattering length of the electron with 50 keV is several hundred angstroms, and hence for the reflection type of diffraction with glancing angles of ~3°, the electron can penetrate the iron oxide layer to only a few tens of angstroms in depth from the surface. A degree of orientation on the surface is expected to be more

TABLE II

X-RAY DIFFRACTION DATA ON VACUUM DEPOSITED THIN ALUMINUM FILM

h k l	d^{obs} (Å)	d^{calc} (Å)	I^{obs}	I^{ideal}		$I^{ideal'a}$		I^{pref} $h = 0.029$ $b = 0.0$		$I^{pref'a}$ $h = 0.029$ $b = 0.0$		$\phi°$	p
1 1 1	2.340	2.3380	100.0	25.0	100.0	25.0	100.0	95.6	100.0	95.6	100.0	0.00	2
1 1 −1				75.0		75.0		4.4		4.4		70.53	6
2 0 0	2.027	2.0248	12.7		47.7		41.3		14.7		12.7	54.74	6
2 2 0	1.433	1.4317	12.5	14.5	29.0	8.9	17.8	19.4	19.5	11.9	11.9	35.26	6
2 −2 0				14.5		8.9		0.1		<0.1		90.00	6
3 1 1	1.222	1.2210	8.4	8.0	32.0	4.2	16.8	14.7	18.2	7.7	9.6	29.50	6
3 1 −1				16.0		8.4		3.4		1.8		58.52	12
3 −1 −1				8.0		4.2		0.1		0.1		79.98	6
2 2 2	1.169	1.1690	4.9	2.3	9.1	1.1	4.6	8.7	9.1	4.4	4.6	0.00	2
2 2 −2				6.8		3.4		0.4		0.2		70.53	6
4 0 0	—	1.0124	—		4.4		1.9		1.3		0.6	54.74	6
R factor					0.57		0.31		0.17		0.015		

[a] Thickness correction was made, noted prime.

enhanced than that in the inner part of the oxide because an oxidation reaction is a diffusion-controlled one, and then the O_2 concentration gradient is highest on the surface. This is the reason why the h factor is higher in the reflection type of diffraction than in the transmission type.

The T.P.T. can also be applied to the

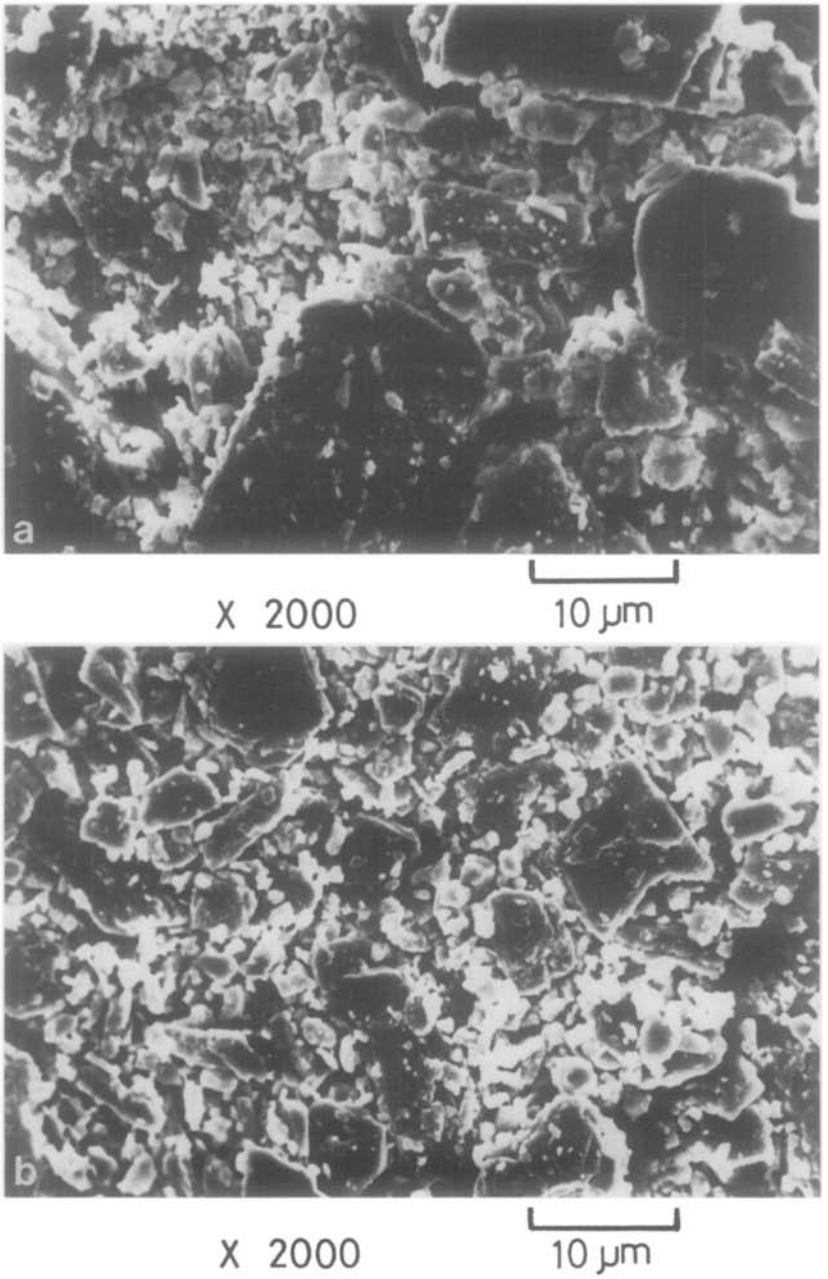

FIG. 6. Secondary electron micrographs for $CaSO_4 \cdot 2H_2O$. (a) As received and (b) recrystallized in water.

polycrystalline samples of very small thickness using X-ray diffraction. Table II shows X-ray diffraction data obtained from an Al film of 1 μm thickness, which was vacuum deposited on the reflectionless sample tray made of a Si single crystal. Every observed intensity is weaker than the ideal one except for the 111 reflection. Inspection of the observed intensity distribution suggests the compatibility of this pattern with the uniaxially oriented one which is characterized with the *hhh* plane. Here the *R* factor was 16.7%. If the film is thick enough, the intensity ratios I^{obs}/I^{ideal} for all the *hhh* planes are 1.0. However, the ratios are smaller than 1.0 in higher-order reflections. Then we have to use Eq. (6) in this case instead of Eq. (4). The *R* factor reduced to only 1.5%.

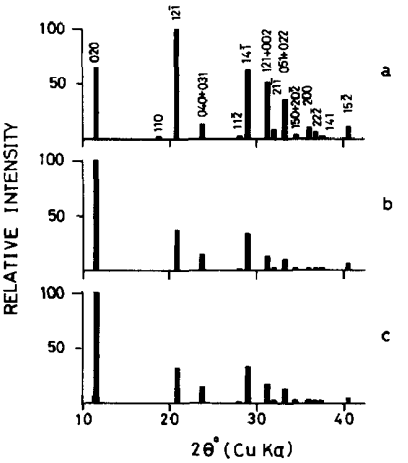

FIG. 8. Schematic X-ray diffraction patterns for $CaSO_4 \cdot 2H_2O$ (recrystalized). (a) Calculated intensities for ideally dispersed powders, $R = 1.01$ compared with (b); (b) observed intensities; and (c) calculated intensities for preferentially oriented powders with $h = 0.036$ and $b = 0.20$, $R = 0.06$ compared with (b).

V. Practical Applications

$CaSO_4 \cdot 2H_2O$ powders available commercially have growth habits which are of two-dimensional shapes, as shown in Fig. 6a. The powders reduce their sizes through recrystallization in water, and hence it becomes difficult to align their orientation planes parallel to a pressurized plane, as shown in Fig. 6b. From these two speci-

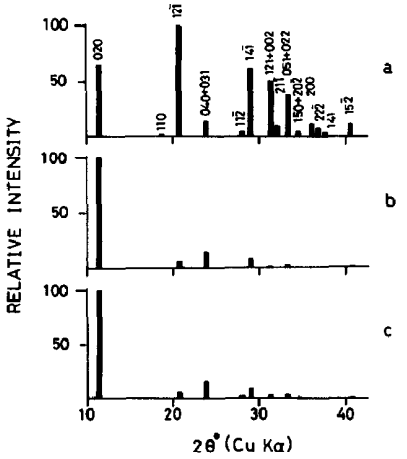

FIG. 7. Schematic X-ray diffraction patterns for $CaSO_4 \cdot 2H_2O$ (as received). (a) Calculated intensities for ideally dispersed powders (*8*), $R = 2.39$ compared with (b); (b) observed intensities; and (c) calculated intensities for preferentially oriented powders with $h = 0.047$ and $b = 0.03$, $R = 0.05$ compared with (b).

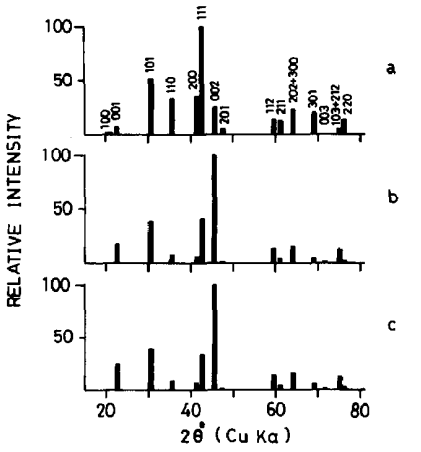

FIG. 9. Schematic X-ray diffraction patterns for $SmCo_5$. (a) Calculated intensities for ideally dispersed powders (*9*), $R = 1.03$ compared with (b); (b) observed intensities; and (c) calculated intensities for preferentially oriented powders with $h = 0.033$ and $b = 0.06$, $R = 0.09$ compared with (b).

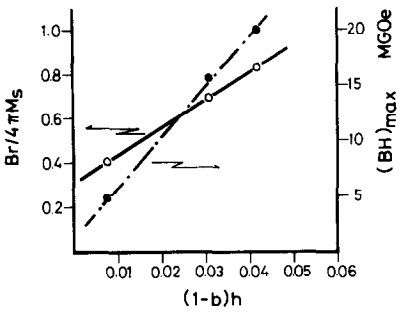

FIG. 10. Relationship between magnetic hardness and degrees of crystallographic orientation.

mens diffraction patterns with different degrees of orientation were obtained, which are shown in Figs. 7 and 8. The former is highly oriented, $h = 0.047$ and $b = 0.03$, and the latter is poorly oriented, $h = 0.036$ and $b = 0.20$, respectively. Thus the quantitative estimation of the degree of orientation is easier and more accurate in the T.P.T. than in the electron micrograph.

An alignment of a magnetically hard axis is essential to make a permanent magnet with high quality, which is made of an aggregate of polycrystals. $SmCo_5$ is a typical permanent magnet of a hexagonal structure, whose magnetic hard axis is 00*l*. A diffraction pattern taken from $SmCo_5$ sin-

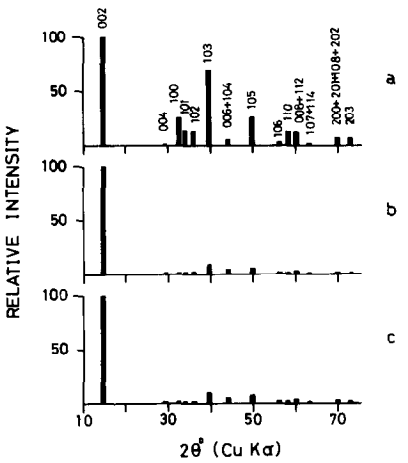

FIG. 12. Schematic X-ray diffraction patterns for MoS_2. (a) Calculated intensities for ideally dispersed powders (*8*), $R = 1.22$ compared with (b); (b) observed intensities; and (c) calculated intensities for preferentially oriented powders with $h = 0.031$ and $b = 0.09$, $R = 0.03$ compared with (b).

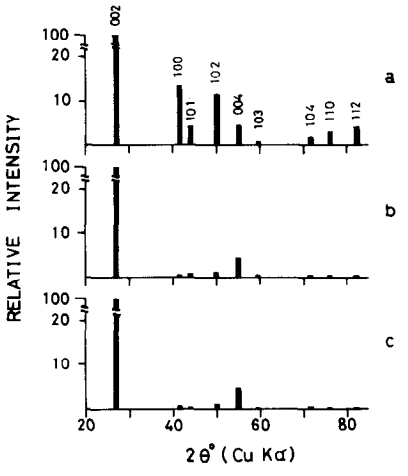

FIG. 11. Schematic X-ray diffraction patterns for BN. (a) Calculated intensities for ideally dispersed powders (*8*), $R = 0.33$ compared with (b); (b) observed intensities; and (c) calculated intensities for preferentially oriented powders with $h = 0.031$ and $b = 0.05$, $R = 0.01$ compared with (b).

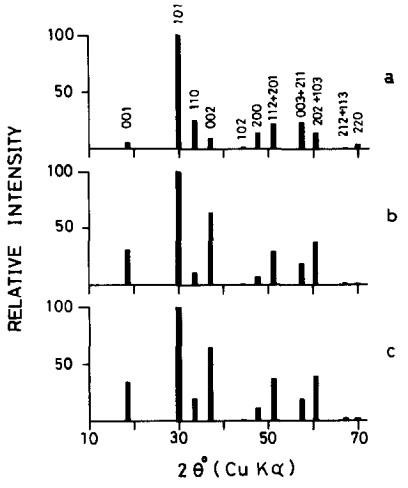

FIG. 13. Schematic X-ray diffraction patterns for tetragonal SnO. (a) Calculated intensities for ideally dispersed powders (*8*), $R = 0.46$ compared with (b); (b) observed intensities; and (c) calculated intensities for preferentially oriented powders with $h = 0.034$ and $b = 0.11$, $R = 0.06$ compared with (b).

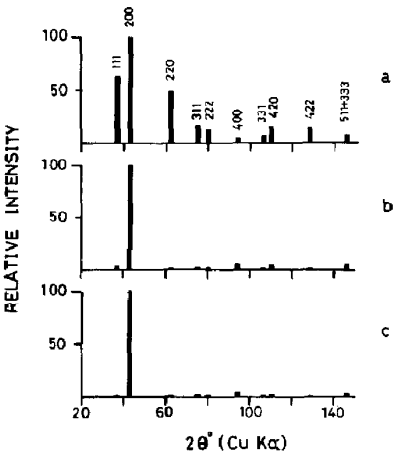

FIG. 14. Schematic X-ray diffraction patterns for NiO. (a) Calculated intensities for ideally dispersed powders (*8*), $R = 1.47$ compared with (b); (b) observed intensities; and (c) calculated intensities for preferentially oriented powders with $h = 0.049$ and $b = 0.00$, $R = 0.040$ compared with (b).

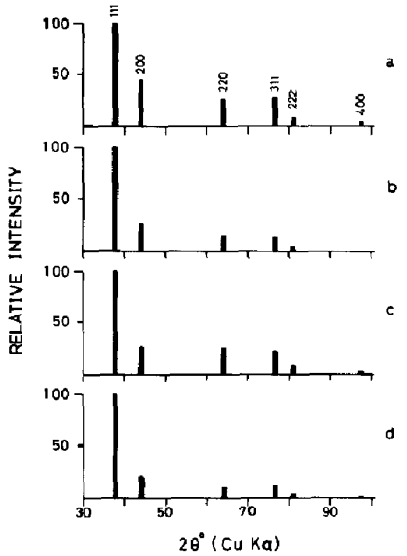

FIG. 15. Schematic X-ray diffraction patterns for vacuum evaporated Ag. (a) Calculated intensities for ideally dispersed powders (*8*), $R = 0.35$ compared with (b); (b) observed intensities; (c) calculated intensities for preferentially oriented powders with $h = 0.023$ and $b = 0.00$, $R = 0.19$ compared with (b); and (d) calculated intensities taken into account of preferred orientation and thickness effect, $h = 0.023$ and $b = 0.00$, $R = 0.01$ compared with (b).

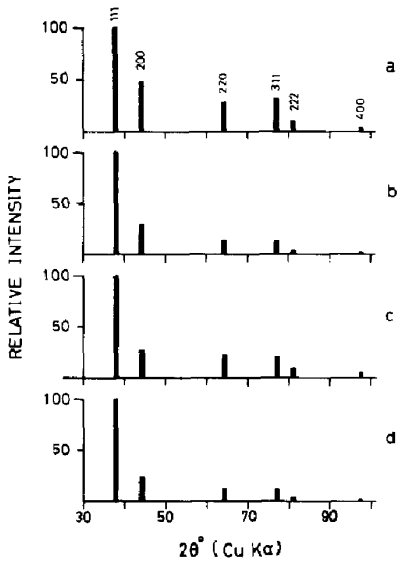

FIG. 16. Schematic X-ray diffraction patterns for vacuum evaporated Au. (a) Calculated intensities for ideally dispersed powders (*8*), $R = 0.35$ compared with (b); (b) observed intensities; (c) calculated intensities for preferentially oriented powders with $h = 0.022$ and $b = 0.00$, $R = 0.22$ compared with (b); and (d) calculated intensities taken into account of preferred orientation and thickness effect, $h = 0.022$ and $b = 0.00$, $R = 0.01$ compared with (b).

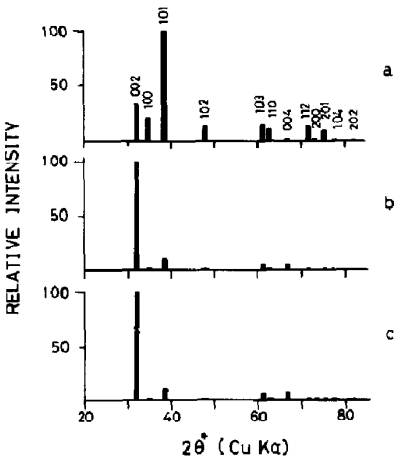

FIG. 17. Schematic X-ray diffraction patterns for electro-deposited Cd. (a) Calculated intensities for ideally despersed powders (*8*), $R = 1.73$ compared with (b); (b) observed intensities; and (c) calculated intensities taken into account of preferred orientation and thickness effect, $h = 0.043$ and $b = 0.04$, $R = 0.02$ compared with (b).

tered anisotropically is shown in Fig. 9, from which a degree of orientation is determined to be $h = 0.033$ and $b = 0.06$. From a series of $SmCo_5$ samples with different degrees of orientation, we can deduce a relationship between magnetic and crystallographic orientation degrees, which are expressed as $B_r/4\pi M_s$ or $(BH)_{max}$, and $h(1 - b)$, respectively (*7*). Here B is magnetization, B_r is remanent magnetization, $4\pi M_s$ is saturation magnetization, and H is magnetic field. The open circles in Fig. 10 stand for $B_r/4\pi M_s$ and the solid ones represent $(BH)_{max}$. The linear relationship between the degrees of magnetic and crystallographic orientations can be found in the figure.

Other examples are shown in Figs. 11–17 for pressed powders of BN, MoS_2 and SnO, nickel monoxide on Ni plate, evaporated thin films of Ag and Au on Si, and an electrodeposited film of Cd, respectively. The agreement between observed and calculated diffraction intensities is satisfactory for these two-dimensional polycrytals. Thus the T.P.T. is applicable to many types of aggregates with two-dimensional shapes or uniaxial orientation.

References

1. F. K. LOTGERING, *J. Inorg. Nucl. Chem.* **9,** 113 (1959).
2. M. UDA, *Z. Anorg. Allg. Chem.* **350,** 105 (1967).
3. M. UDA, *Z. Anorg. Allg. Chem.* **361,** 94 (1968).
4. Y. SASA AND M. UDA, *J. Solid State Chem.* **18,** 63 (1976).
5. T. SAKURAI (Ed.), "Universal Crystallographic Computation Program System," The Crystallogr. Soc. Japan, Tokyo (1967); G. YAMAGUCHI AND H. MIYABE, *Ceram. Japan* **9,** 176 (1974).
6. L. KIHLBORG, *Ark. Kemi* **21,** 357 (1963).
7. Y. SASA AND M. UDA, *Yogyo-Kyokaishi* **88,** 316 (1980).
8. RALPH W. G. WYCKOFF, "Crystal Structures," 2nd ed., Interscience, New York, (1963).
9. Y. KHAN AND D. FELDMANN, *J. Less-Common Met.* **31,** 211 (1973).